Nano-Micro Letters

e-ISSN 2150-5551
CN 31-2103/TB

ARTICLE

https://doi.org/10.1007/s40820-025-01985-w

Cite as
Nano-Micro Lett.
(2026) 18:132

Received: 2 July 2025
Accepted: 11 October 2025

Tri-Band Regulation and Split-Type Smart Photovoltaic Windows for Thermal Modulation of Energy-Saving Buildings in All-Season

Qian Wang[1], Zongxu Na[1], Jianfei Gao[1], Li Yu[2] ✉, Yuanwei Chen[1], Peng Gao[3], Yong Ding[4] ✉, Songyuan Dai[5], Mohammad Khaja Nazeeruddin[6] ✉, Huai Yang[7] ✉

HIGHLIGHTS

- Broadening the modulation range and decreasing the driving voltage of polymer dispersed liquid crystals via molecular engineering without sacrificing high solar transmittance (transparent state) and solar modulating ability.
- Modulating capability of the smart photovoltaic windows across visible, near-infrared and mid-infrared bands enabling superb energy-saving performance in all season.
- Holding a great potential for real-world application due to their scalable manufacturing technology.

ABSTRACT Energy-saving buildings (ESBs) are an emerging green technology that can significantly reduce building-associated cooling and heating energy consumption, catering to the desire for carbon neutrality and sustainable development of society. Smart photovoltaic windows (SPWs) offer a promising platform for designing ESBs because they present the capability to regulate and harness solar energy. With frequent outbreaks of extreme weather all over the world, the achievement of exceptional energy-saving effect under different weather conditions is an inevitable trend for the development of ESBs but is hardly achieved via existing SPWs. Here, we substantially reduce the driving voltage of polymer-dispersed liquid crystals (PDLCs) by 28.1 % via molecular engineering while maintaining their high solar transmittance (T_{sol} = 83.8 %, transparent state) and solar modulating ability (ΔT_{sol} = 80.5 %). By the assembly of perovskite solar cell and a broadband thermal-managing

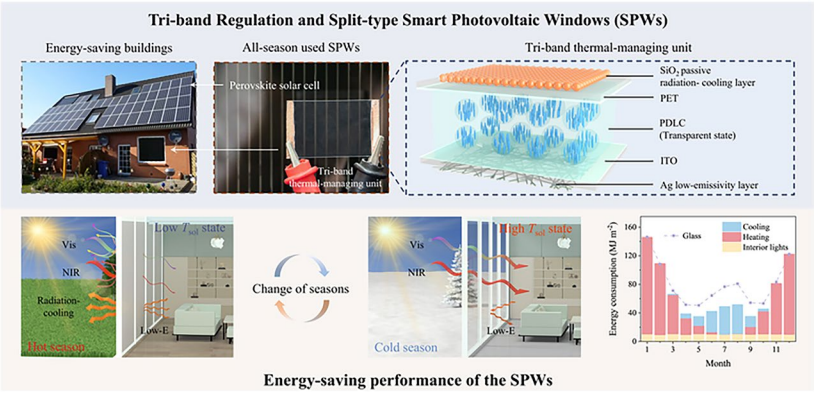

✉ Li Yu, li.yu@wit.edu.cn; Yong Ding, yding@hhu.edu.cn; Mohammad Khaja Nazeeruddin, mdkhaja.nazeeruddin@epfl.ch; Huai Yang, yanghuai@pku.edu.cn

[1] Institute for Advanced Materials and Technology, University of Science and Technology Beijing, Beijing 100083, People's Republic of China
[2] State Key Laboratory of Green and Efficient Development of Phosphorus Resources, Hubei Key Laboratory of Plasma Chemistry and Advanced Materials, School of Materials Science and Engineering, Wuhan Institute of Technology, No. 206 Guanggu 1 Road, Wuhan 430205, People's Republic of China
[3] Fujian Institute of Research on the Structure of Matter, Chinese Academy of Sciences, Fuzhou 350002, People's Republic of China
[4] College of Renewable Energy, Hohai University, Changzhou 213000, People's Republic of China
[5] Beijing Key Laboratory of Novel Thin-Film Solar Cells, School of New Energy, North China Electric Power University (NCEPU), Beijing 102206, People's Republic of China
[6] Institute of Chemical Sciences and Engineering, École Polytechnique Fédérale de Lausanne (EPFL), CH-1015 Lausanne, Switzerland
[7] School of Materials Science and Engineering, Peking University, Beijing 100871, People's Republic of China

Published online: 05 January 2026

Shanghai Jiao Tong University Press

Springer

unit encompassing the electrical-responsive PDLCs, transparent high-emissivity SiO_2 passive radiation-cooling, and Ag low-emissivity layers possesses, we present a tri-band regulation and split-type SPW possessing superb energy-saving effect in all-season. The perovskite solar cell can produce the electric power to stimulate the electrical-responsive behavior of the PDLCs, endowing the SPWs zero-energy input solar energy regulating characteristic, and compensate the daily energy consumption needed for ESBs. Moreover, the scalable manufacturing technology holds a great potential for the real-world applications.

KEYWORDS Smart photovoltaic windows; Polymer-dispersed liquid crystals; Passive radiative cooling; Tri-band regulation; Energy-saving buildings

1 Introduction

Building energy consumption approximately occupies 30 % of global energy [1, 2]. With frequent outbreaks of extreme weather all over the world, the building-associated cooling and heating energy consumption increases year by year [3]. Energy-saving buildings (ESBs), a green technology capable of effectively restraining the energy consumption via regulating and harnessing solar energy, emerge as the times require [4].

Windows are the primary medium for the energy exchange between ESBs and external environment [5]. The proportion of windows in modern architecture is gradually increasing [6]. Making windows active to react to the weather condition of external environment affords an effectual avenue for exploiting ESBs [7]. Smart photovoltaic windows (SPWs), as a multifunctional stimuli-responsive device, offer a promising platform for exploring ESBs attributed to their significant features [8, 9]. Their transparency can be dynamically modulated on demand under a variety of external stimuli to enable ESBs the energy-saving effect [10–13]. They are able to directly convert solar energy into electrical energy providing additional energy source for daily consumption of ESBs [14].

To date, the combination of electrical-responsive chromic materials and the photovoltaics has become the mainstream for designing SPWs for several reasons. The electrical-responsive feature enables SPWs to freely modulate solar energy according to the demand of the occupants under complex environments [15–17]. The electric output generated by the photovoltaics via harnessing solar energy is able to be utilized for trigger dynamic solar energy regulating behavior of electrical-responsive chromic materials which endows the SPWs self-driven characteristics, further enhancing their energy-saving performance [18]. In addition, electrical-responsive feature makes SPWs facile to be connected with the computer and internet equipment holding the potential for constructing smart home systems in the future [19].

Diverse electrical-responsive chromic materials including conducting polymers [20, 21], viologens [22, 23], transition metal oxides [24–30], and liquid crystals [31, 32] have been employed as a chromic unit to assemble with the photovoltaics such as organic, dye-sensitized, silicon, and perovskite solar cells for developing SPWs of distinct micro-/macrostructures. Compared to other electrical-responsive chromic materials, polymer-dispersed liquid crystals (PDLCs) have been considered as an ideal candidate for exploiting SPWs because they can be mass manufactured into large-scale flexible films that possess high contrast ratio, fast response speed, and excellent cyclical stability [33]. Reducing the driving voltage and improving the solar modulating ability (ΔT_{sol}) are key issues for real-word application of PDLCs in SPWs [34]. Recently, the doping of nanoparticles, $BaTiO_3$, ZnO, and Ag, into PDLCs is a commonly used and effective strategy for lowering the driving voltage [35–37]. However, the transmittance of PDLCs at transparent state inevitably sacrifices in order to significantly reduce the driving voltage due to scattering effect of the nanoparticles, which is adverse to the realization of extraordinary energy-saving effect in all-season and their wide applications across distinct climate zones [38, 39]. According to the energy distribution of solar irradiation and the spontaneous emission, a broadband regulating capability in the region of visible, near-infrared, and mid-infrared is required for achieving ideal energy-saving performance [40]. For this, previous researches have introduced fluorine-containing monomer into PDLCs to enable dynamic thermal modulating performance in visible and near-infrared area and enhance their passive radiation-cooling effect [41–43]. However, the application of fluorine-containing compounds certainly will cause serious harm to environment and human health [44].

Herein, we remarkably reduce the driving voltage via introducing polar and nonpolar molecules into the PDLCs

 https://doi.org/10.1007/s40820-025-01985-w

while maintaining their high solar transmittance (transparent state) and ΔT_{sol}. A broadband thermal-managing unit (BTMU) is built up by electrical-responsive PDLCs, transparent high-emissivity (H-E_{MIR}) SiO_2 passive radiation-cooling (PRC), and Ag low-emissivity (L-E_{MIR}) layers (Fig. 1a). By assembling the BTMU and perovskite solar cell (Table S1), we present a conceptional demonstration of a tri-band regulation and split-type SPW for all-season ESB thermal regulation. Unlike previously reported SPWs [20–32], our designed SPWs possess broadband modulating ability to visible (380–780 nm), near-infrared (NIR, 780–2500 nm), and mid-infrared (MIR, 8–13 μm) enabling exceptional energy-saving effect in all-season (Fig. 1b). As presented in Fig. 1c, in hot season, the PDLCs at opaque state can efficaciously block the thermal radiation of visible and NIR bands in solar energy into the indoor while SiO_2 layer displays passive radiative cooling effect, which is able to greatly reduce the cooling energy consumption [45, 46]. In cold season, the thermal radiation of visible and NIR bands in solar energy is allowed for entering into the indoor to compensate the energy consumption needed for the heating thanks to high solar transmittance (T_{sol}) of the BTMU when the PDLC is at transparent state (Fig. S1). In addition, Ag L-E_{MIR} layer is beneficial for suppressing the radiative heat exchange between the indoor and outdoor environments in all-season further elevating the energy-saving effect of the SPWs [47]. Besides superb energy-saving performance in different seasons, two significant features make our designed SPWs broad prospects in ESBs. The perovskite solar cell is capable of providing the SPWs high photoelectric conversion efficiency (PCE) and powering the stimuli-responsive behavior of the PDLCs by harnessing solar energy. Therefore, tri-band regulation characteristic of the SPWs for achieving energy-saving effect in all-season requires none-energy input. Moreover, the SPWs are potential for industrial mass production because they are manufactured mainly using roll-to-roll and spraying technologies.

2 Experimental Section

2.1 Materials

The polymer monomer and small molecule liquid crystal (SMLC) used for synthesizing the PDLCs were purchased from Yantai Xian Hua Technology Group Co., Ltd. Hydrophobic fumed silica, AEROSIL R812S, was obtained from Evonik. Isopropanol, butyl acetate, ethanol, and tetrahydrofuran (THF) were purchased from Sinopharm Chemical Reagent Co., Ltd. Poly(ethylene-co-acrylic acid) with 15 wt%

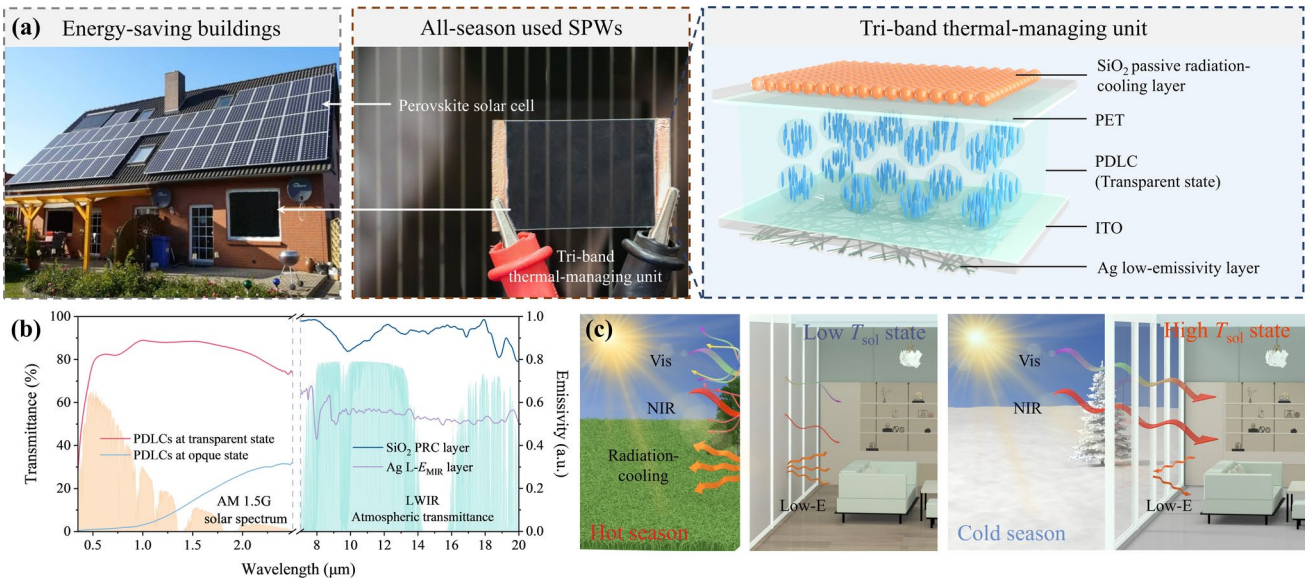

Fig. 1 **a** Photographs of the tri-band regulation and split-type SPWs for all-season used ESBs, along with a diagrammatic sketch illustrating the architecture of the BTMU. **b** Transmittance spectra of (0.38–2.5 μm) of the PDLCs at transparent and opaque states, and MIR emissivity (7.0–20 μm) of the SiO_2 PRC and Ag layers in optimized BTMU. **c** Working principle of the SPWs in hot season (left) and cold season (right)

acrylic acid content (EAA) were purchased from Aladdin. All chemicals were used as received.

2.2 Preparation of Polymer-Dispersed Liquid Crystals (PDLCs)

The polymer monomer, SMLC, photo initiator, and glass micro balloon were well mixed and served as the syrup. The syrup was injected between two conductive PET films. The PDLCs were obtained via roll-to-roll process and exposure to ultraviolet light (365 nm, 15 mW cm^{-2}) for 15 min. The thickness of the PDLCs was 20 μm and controlled by the diameter of the glass micro balloon. The composition of the PDLCs is seen in Table S3. The PDLCs with different concentrations of the POSS were prepared by the similar process in which the POSS was mixed with the polymer monomer, SMLC, photo initiator, and glass micro balloon and served as the syrup (Table S4).

2.3 Preparation of Broadband Thermal-Managing Unit (BTMU)

To make sure good adhesion of SiO_2 passive radiation-cooling and Ag low-emissivity layers to the PDLCs, the EAA, as an adhesive layer, was coated on upper and lower surfaces of the PDLC. Hydrophobic fumed SiO_2 was dispersed in 100 mL isopropanol. To fabricate the BTMU, hydrophobic fumed silica nanoparticles and laboratory-synthesized Ag nanowires were firstly dispersed into the solvent of isopropanol and ethanol, respectively. The concentration of the silica nanoparticle and Ag nanowire dispersion solution was 10 and 3 mg mL^{-1}. The BTMU was prepared by spraying the silica nanoparticle and Ag nanowire dispersion solution on upper and lower surfaces of the PDLCs. The spraying process was conducted using a spray gun with the pressure of 0.2 MPa and moving speed of 7 cm s^{-1}, following a line-to line fashion.

2.4 Characterizations

The Vis–NIR transmittance spectra for all samples were measured by using a UV–Vis–NIR spectrophotometer (PerkinElmer, Lambda 1050+). The solar transmittance (T_{sol}) is calculated as follows:

$$T_{sol} = \frac{\int_{0.3\mu m}^{2.5\mu m} T(\lambda)\psi_{sol}(\lambda)d\lambda}{\int_{0.3\mu m}^{2.5\mu m} \psi_{sol}(\lambda)d\lambda} \quad (1)$$

where $T(\lambda)$ is the measured spectral transmittance and $\psi_{sol}(\lambda)$ is the spectral solar power (AM1.5G).

The electro-optical properties of the PDLCs were characterized using a LC parameter analyzer (LCT-5016C, Changchun Liancheng Instrument Co., Ltd.). A halogen-based laser source emitting at 550 nm and a 100 Hz square-wave electric field were applied during the measurement. The field emission scanning electron microscope (FE-SEM, Carl Zeiss, SUPRA 55 SAPPHIRE) was used to characterize the microstructure of the PDLCs, high-emissivity (H-E_{MIR}) SiO_2 passive radiation-cooling (PRC) and Ag low-emissivity (L-E_{MIR}) layers, and morphology of laboratory-synthesized Ag nanowires.

Emissivity curves across the 2.5–25 μm spectral band were measured via a FTIR spectrometer (INVENIO-S, Bruker) integrated with a gold-plated integrating sphere. Following Kirchhoff's radiation principle, which states $\alpha(\lambda) = \varepsilon(\lambda)$ at thermal equilibrium, the emissivity was calculated using $\varepsilon(\lambda) = 1 - \rho(\lambda) - \tau(\lambda)$. The infrared camera (FLIR E54) was used to characterize the passive radiation-cooling effect of the SiO_2 passive radiation-cooling PRC layer and heat insulation performance of the Ag L-E_{MIR} layer.

2.5 Energy-Saving Performance Simulation

In EnergyPlus, a model house measuring 8 m (L) × 8 m (W) × 3 m (H) was established, with 4 m × 2 m windows centrally located on each wall, resulting in a window-to-wall ratio of 33 % (Fig. S15). The heating and cooling energy consumption was modeled using EnergyPlus whole-building energy simulation by applying an "ideal-loads-air-system" supplied by district cooling and heating sources. For cooling, the indoor temperature was maintained at 24 °C, and for heating, it was maintained at 22 °C. An air change rate 0.3 ACH (air changes per hour), which is consistent with the requirement of both ASHRAE 90.1 and ASHRAE 62.1 standards, was selected as the air infiltration parameter. The annual electricity generation of perovskite solar cell was calculated using EnergyPlus built-in photovoltaic function, with the area set to 50 % of the roof area, a conversion efficiency of 16 %, and a transmission efficiency of 98 %. In the carbon emission calculations, the carbon emission factor for

 https://doi.org/10.1007/s40820-025-01985-w

electricity was set to 0.84 $kgCO_2$ kWh^{-1}, and for natural gas, it was set to 0.056 $kgCO_2$ MJ^{-1}.

3 Results and Discussion

3.1 Modulation the Electro-Optical Properties of PDLCs via Molecular Engineering

To prove our concept, we initially fabricate low-voltage driven, fast response, fatigue resistant, and visible and NIR modulable PDLCs by utilizing acrylate containing hydroxyl group (A-HG) and E8 as the polymer monomer and small molecule liquid crystal (SMLC) through roll-to-roll technology (Fig. 2a). Under external electric field, the PDLCs can reversibly switch between transparent and opaque states due to the alteration of the alignment of the SMLC (Fig. 2b and Movie S1) [48, 49]. As presented in Figs. 2c, S2a and Movie S2, the PDLCs exhibit low T_{sol} at initial state (opaque state) because randomly aligned SMLC leads the mismatch in refractive indexes between the polymer matrix and SMLC [50]. On the contrary, the PDLCs display high T_{sol} as applying voltage (transparent state) because the external electric field can induce vertical alignment of the SMLC making the ordinary refractive index of the SMLC match with the refractive index of the polymer matrix [51]. Obviously, the content of the A-HG has a significant impact on the T_{sol} of the PDLCs at both transparent and opaque states that determines their solar modulating ability (ΔT_{sol}) (Fig. S2b, c) [52]. When the content of the A-HG is lower than 10.05 wt%, the transmittance of the PDLCs in visible region apparently improves while that of the PDLCs in NIR region clearly drops with the increasing content of the A-HG owing to the reduction of the size of SMLC droplets (Figs. 2e-(i-iv) and S3) [53]. The smaller size of the SMLC droplets is, the higher saturation voltage (V_{sat}, driving voltage) is required for inducing vertical alignment of the SMLC in the PDLCs because of higher anchoring energy exerted on the SMLC resulting from increased interaction area between the SMLC droplets and polymer matrix (Fig. 2d) [54]. When the content of the A-HG further increases to 13.43 wt%, the SMLC, as a continuous phase instead of the droplets, disperses in the PDLCs which greatly sacrifices the ΔT_{sol} and raises the driving voltage of the PDLCs (Fig. 2d, e-v). Although the PDLCs possess outstanding ΔT_{sol} of 79.49 % as the content of the A-HG is 10.05 wt%, the driving voltage of 28.1 V is relatively higher which is inconvenient to integrate with perovskite solar cell for realizing the self-powered feature. In order to diminish the driving voltage of the PDLCs, and meanwhile maintain excellent solar modulating ability, a cage-molecule polyhedral oligomeric silsesquioxane (POSS) is introduced into the PDLCs (Fig. S4). As presented in Figs. 2f and S5a, the driving voltage of the PDLCs substantially declines from 28.1 to 20.2 V as the concentration of the POSS is 3 wt% because the incorporation of the nonpolar POSS with low surface energy can decrease the anchoring energy of the polymer matrix to the SMLC and enhance the steric repulsion between the SMLC and polymer matrix (Fig. S5b) [55, 56]. Simultaneously, the ΔT_{sol} of the PDLCs is as high as 80.5 % when the concentration of the POSS is 3 wt% indicating that the addition of the POSS does not sacrifice the solar modulating ability because original microstructure of the PDLCs and size of the SMLC droplets are well retained (Figs. 2g and S5c, d). The high ΔT_{sol} is promising for providing SPWs superb energy-saving performance (Table S2). Thanks to the low driving voltage of the PDLCs, perovskite solar cell is capable of affording a steady output voltage to stimulate the electrical-responsive behavior of the PDLCs during the day time for providing the energy-saving effect (Figs. 2h, S6, and Movie S3). Last but not the least, the PDLCs exhibit fast response characteristic, excellent cyclical, and environmental stability that are important for their practical application (Figs. S7, S8 and Movie S4). Notably, 95.2 % initial power conversion efficiency of the perovskite solar cell still retains after it powers the transparency switching behavior of the PDLCs for 1500 cycles (Fig. S9).

3.2 Construction and Optimization of Mid-Infrared Radiation Modulation Layers

To endow with the SPWs ideal energy-saving effect in all-season which is hardly achieved in the existing SPWs [20–32], a BTMU encompassing the electrical-responsive PDLC, H-E_{MIR} SiO_2 PRC layer, and Ag L-E_{MIR} layer is designed according to broadband thermal radiation of solar energy and fabricated by coating the SiO_2 nanoparticles and Ag nanowires on upper and lower surfaces of the PDLCs via spraying technology (Fig. 3a). Herein, SiO_2 nanoparticles are selected to build up the PRC layer because of their low absorbance in visible and NIR region, H-E_{MIR} in MIR region,

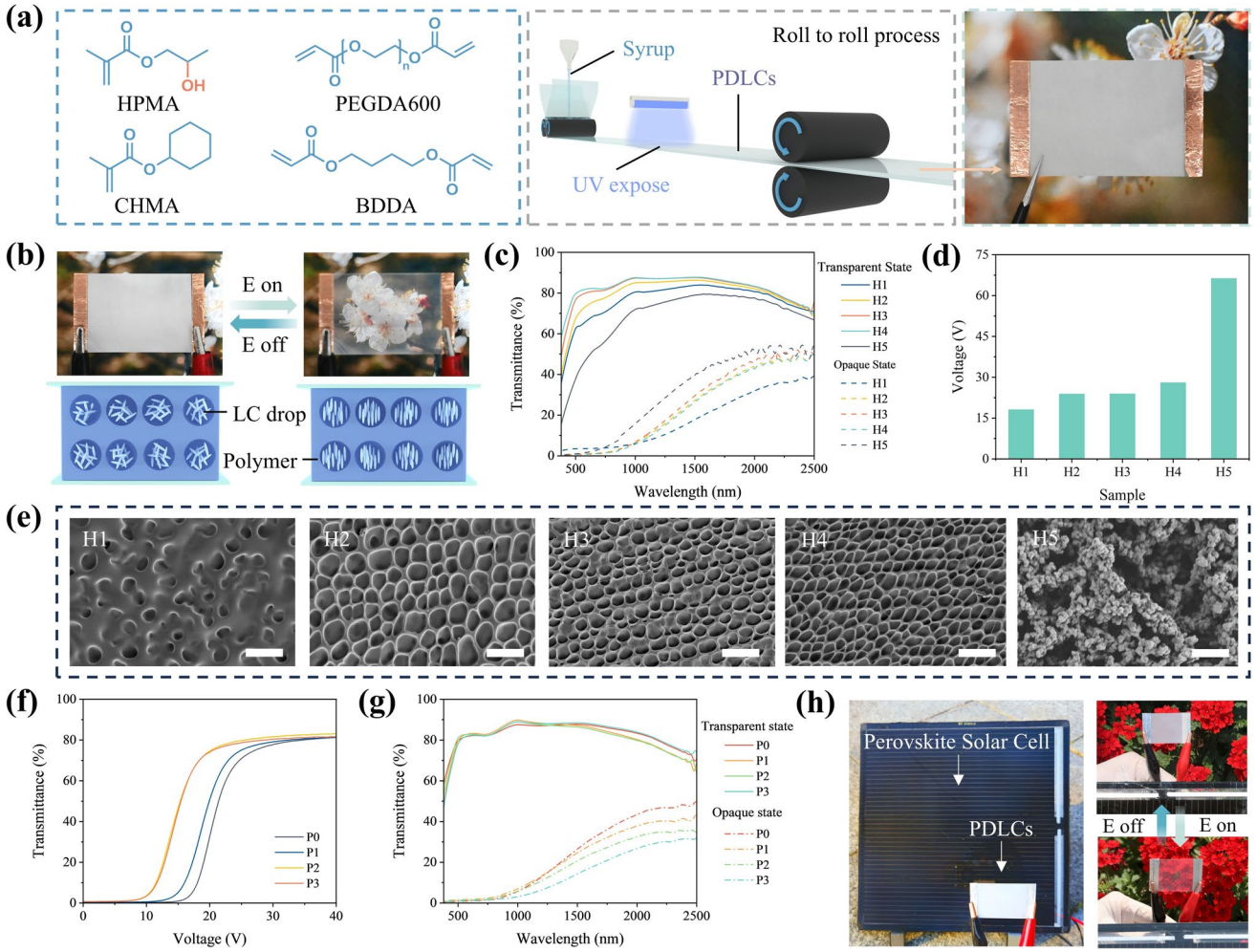

Fig. 2 **a** Chemical structure of the polymer monomer using for fabricating low-voltage driven, fast response, fatigue resistant, and visible and NIR modulable PDLCs (left). Schematic illustration of the roll-to-roll technology for fabricating the PDLCs (middle). Photograph of as-prepared PDLCs (right). **b** Photographs of the PDLCs under the voltage of 0 V and 30 V (top). Schematic illustration of the alignment of the SMLC in the PDLCs at transparent and opaque states (bottom). **c** Transmittance spectra of (0.38–2.5 μm) of the PDLCs with different contents of the A-HG at transparent (0 V) and opaque states (30 V). **d** Saturation voltage (V_{sat}, driving voltage) and **e** scanning electron microscope (SEM) images of the PDLCs with different contents of the A-HG. The scale bar is 6 μm. **f** Electro-optical curve of the PDLCs with different contents of the POSS. **g** Transmittance spectra of (0.38–2.5 μm) of the PDLCs with different contents of the POSS at transparent (0 V) and opaque states (30 V). **h** Self-powered feature of the PDLCs

and modulable microstructure [57, 58]. The laboratory-synthesized Ag nanowires are employed to fabricate the L-E_{MIR} layer originates because it is facile to form the microstructure of high transparence in visible and NIR region and high reflectance in MIR region based on them (Fig. S10) [59, 60]. In our design, the working principle of the BTMU offering the SPWs energy-saving effect is based on the regulating capability of its three key components to solar energy. In hot season, the PDLCs at opaque state effectively block visible and NIR light entering into the indoor and H-E_{MIR} SiO_2 PRC layer continuously radiates the heat through atmospheric window (8–13 μm), which can significantly reduce the energy consumption needed for the air-conditioning. In cold season, high T_{sol} of the BTMU (the PDLCs is at transparent state) is conducive to the thermal radiation of solar energy into the indoor, and thus saving the energy consumption demanded for the heating. In both hot and cold seasons, the Ag L-E_{MIR} layer can curb the radiative heat exchange between the indoor and outdoor environments further enhancing the energy-saving effect of the SPWs. Consequently, SiO_2 PRC layer of high H-E_{MIR} and T_{sol} and Ag layer of L-E_{MIR} and high T_{sol} are required for enabling SPWs superb energy-saving effect in

 https://doi.org/10.1007/s40820-025-01985-w

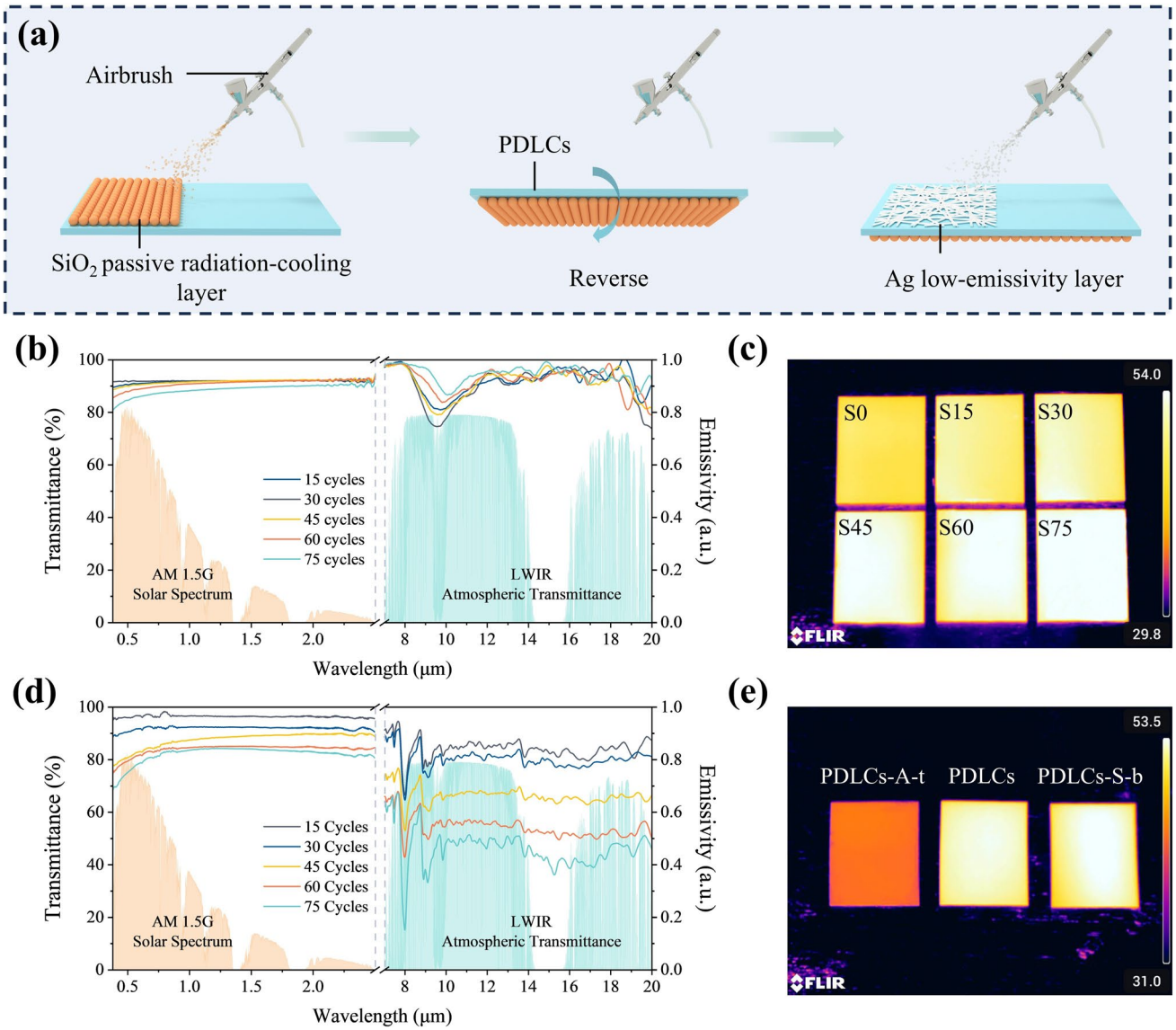

Fig. 3 **a** Schematic illustration of the spraying technology for fabricating the BTMU. **b** Transmittance spectra of (0.38–2.5 μm) and MIR emissivity (7.0–20 μm) of the SiO_2 PRC layer prepared by different spraying cycle numbers. **c** IR images of the SiO_2 PRC layer of different spraying cycle numbers on a hot stage with the temperature of 60 °C. **d** Transmittance spectra of (0.38–2.5 μm) and MIR emissivity (7.0–20 μm) of Ag L-E_{MIR} layer prepared by different spraying cycle numbers. **e** IR images of PDLCs with top surface coated by Ag L-E_{MIR} layer (60 spraying cycles, PDLCs-A-t), PDLCs, and PDLCs with bottom surface coated by SiO_2 PRC layer (60 spraying cycles, PDLCs-S-b) on a hot stage with the temperature of 60 °C

all-season. As presented in Figs. 3b, c, and S11a, the increment of the number of spraying cycles can raise the E_{MIR} of the SiO_2 PRC layer caused by the augment of the absorption coefficient, and resulting in the rise of the radiative cooling effect [61]. However, larger number of spraying cycles inevitably lead the formation of SiO_2 agglomerates in micrometer size which lowers the T_{sol} of the SiO_2 PRC layer because of the scattering effect (Figs. 3b and S11b, c). Similarly, growing number of spraying cycles can diminish the E_{MIR} of Ag layer enhancing the heat-retaining capacity but sacrifice the T_{sol} owing to the denser structure (Figs. 3d, e, and S12) [62]. To balance the trade-off between the E_{MIR} and T_{sol} of the SiO_2 PRC and Ag layers for giving the SPWs optimized energy-saving effect in both hot and cold seasons, the SiO_2 PRC and Ag layers made from 60 spraying cycles are finally utilized to integrate with the PDLCs for the construction of

the BTMU. To elucidate operational stability of the SPWs for real-world application, a series of accelerated aging tests are performed on the SiO_2 PRC and Ag layers. The E_{MIR} of the SiO_2 PRC and Ag layers almost retain for the accelerated aging tests, proving their superior environmental stability (Fig. S13).

3.3 Energy-Saving Potential Simulation of SPWs

For evaluating the energy-saving performance of the SPWs, a small "house" is built up by utilizing an aluminum foil wrapped polystyrene foam box and BTMU as the main body and window, respectively (Fig. 4a). The chamber in the polystyrene foam box can be considered as the indoor environment. Its temperature is recorded by a K-type thermocouple. In order to minimize the thermal conduction and convection between the indoor and external environments, the polystyrene foam box is sealed by a polyethylene film. In addition, xenon and infrared lamps are applied for emulating sunlight. As presented in Fig. 4b, the chamber temperature sharply goes up and reaches as high as $T_{BTMU,\ HT\text{-}IX} = 51.3$ °C under the illumination of the xenon lamp when the BTMU exhibits high T_{sol}. When removing the xenon lamp, the chamber temperature gradually decreases to $T_{BTMU,\ HT\text{-}N} = 25.1$ °C. The large difference of the chamber temperature between the illuminating and nonilluminating states demonstrates exceptional energy-saving effect of the SPWs in cold season. Under the same irradiation condition, the chamber temperature can greatly reduce from $T_{BTMU,\ HT\text{-}IX} = 51.3$ °C to $T_{BTMU,\ LT\text{-}IX} = 47.0$ °C as the BTMU presents low T_{sol} verifying superb energy-saving effect of the SPWs in hot season. To validate the PRC effect of H-E_{MIR} SiO_2 layer and heat insulation function of the Ag L-E_{MIR} layer, the PDLCs are also employed as the window as the reference. Attributed to the heat insulation function of the Ag L-E_{MIR} layer, up on exposure to xenon lamp, the chamber temperature rises from the room temperature to $T_{PDLCs,\ HT\text{-}IX} = 49.8$ °C that is lower than $T_{BTMU,\ HT\text{-}IX} = 51.3$ °C although the T_{sol} of PDLCs is higher than that of the BTMU [63]. Under the illumination of the xenon lamp, the chamber temperature is $T_{PDLCs,\ LT\text{-}IX} = 47.0$ °C, which is 3.2 °C higher than $T_{BTMU,\ LT\text{-}IX} = 43.8$ °C when the PDLCs are at opaque state. As a result, the chamber temperature is able to further reduce as irradiated by the xenon lamp with the help of the PRC effect of H-E_{MIR} SiO_2 layer. Obviously, the H-E_{MIR} SiO_2 and Ag L-E_{MIR} layers take an essential role in giving the SPWs distinguished energy-saving performance in all-season which is furthered proved in the investigation of the energy-saving effect of the SPWs using an infrared lamp as the solar simulator (Fig. 4c). As Beijing is a large city with great energy consumption, it is chosen as the location of the simulation for energy-saving evaluation (more details about the simulation are given in Experimental Section). With the normal glass as the baseline, the designed SPWs can save 16.7 % of the annual building energy consumption for the heating and air-conditioning (Fig. 4d). In our designed SPWs, the perovskite solar cell is capable of generating the electric energy to stimulate the high T_{sol} state of the BTMU, promising the thermal irradiation of solar energy into the indoor and significantly diminishing the heating energy consumption needed in cold season. In hot season, original low T_{sol} state of the BTMU is able to effectively hinder the thermal irradiation of solar energy, greatly reducing the energy consumption required for air-conditioning. Therefore, the electric energy produced by the SPWs can be used for daily energy consumption of the ESBs. According to the working mode of the SPWs, the annual average power generation of the SPWs is estimated to be 1.76×10^4 kWh (Fig. 4e). Benefitting from the energy-saving and electric power generation characteristics, the application of the SPWs in the ESBs can approximately reduce 16.9 tons of carbon emissions every year (Fig. 4f). To investigate the effect of the climate condition on the energy-saving performance of our designed SPWs, Oslo, a city of typical temperate marine climate located at high-latitude region, is also selected as the location for the simulation. As presented in Fig. S14a, the designed SPWs can save 7.3 % of the annual building energy consumption. The attenuation of the energy-saving performance for Oslo mainly originates from two reasons. The temperature of Oslo through the year is lower than that of Beijing, especially in hot season. In addition, the solar radiation of Oslo is less than that of Beijing due to the geographic location and climate condition of Oslo, which is proved by annual average power generation of the two cities (Oslo, 1.15×10^4 kWh and Beijing, 1.76×10^4 kWh) (Figs. 4e and S14b). The SPWs can reduce around 10.7 tons of carbon emissions every year as they are employed in Oslo (Fig. S14c).

https://doi.org/10.1007/s40820-025-01985-w

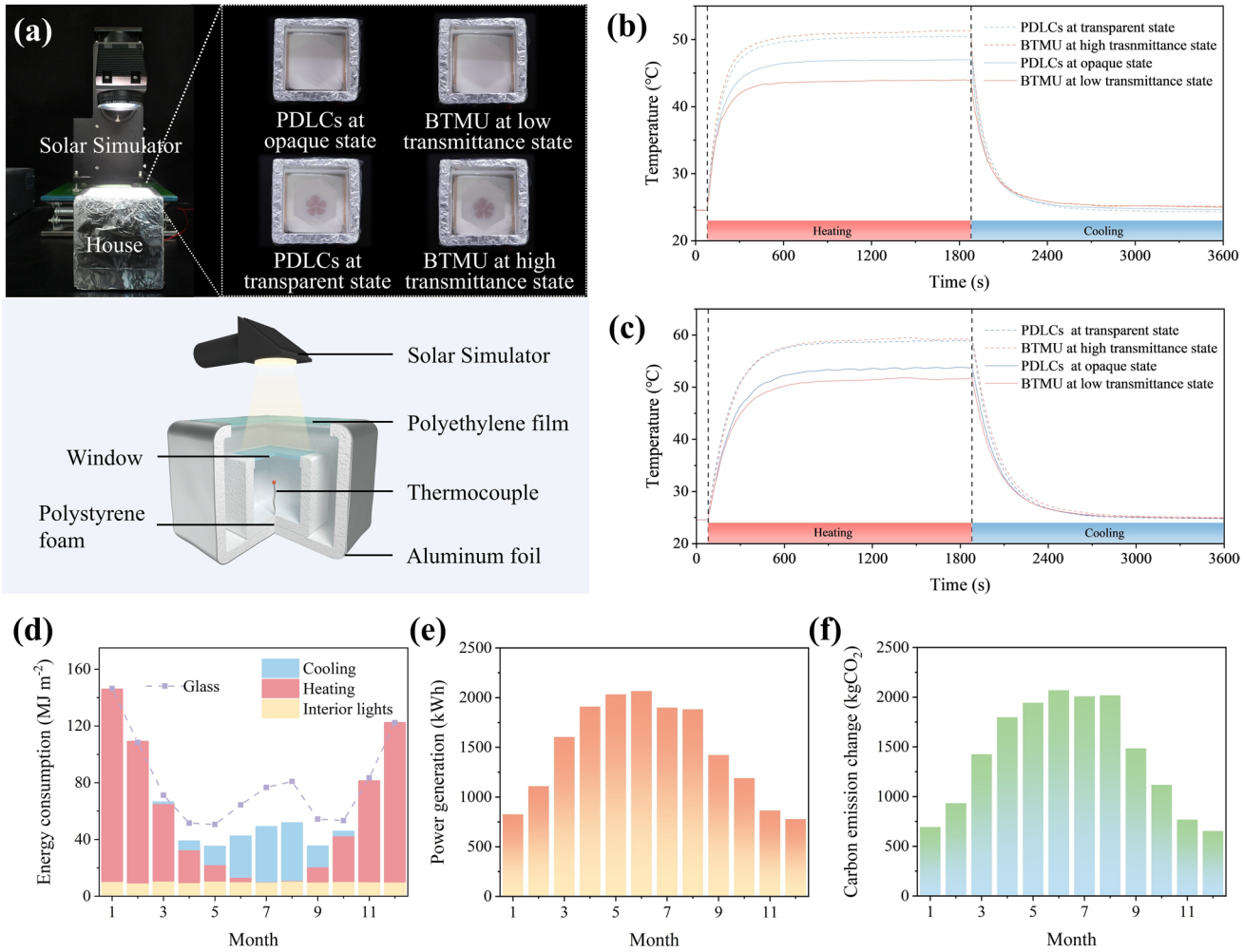

Fig. 4 **a** Photograph and diagrammatic sketch of the apparatus for evaluating the energy-saving performance of the SPWs. Chamber temperature variation curves during the process of solar irradiation and unirradiation under different states of the window (BTMU and PDLCs) when utilizing using **b** xenon and **c** infrared lamps as the solar simulator (HT: high T_{sol} state; LT: low T_{sol} state; IX: illumination by the xenon lamp; N: non illumination). **d** Monthly energy consumption of the SPWs and normal glass window in the climate condition of Beijing. **e** Monthly power generation of the SPWs according the working mode of the SPWs. **f** Monthly saving carbon dioxide emission estimated based on saving energy consumption and power generation of the SPWs

4 Conclusions

In summary, we have demonstrated a tri-band regulation and split-type SPW by assembling a BTMU and perovskite solar cell. The BTMU composed of the electrical-responsive PDLC, H-E_{MIR} SiO_2 PRC and Ag L-E_{MIR} layers presents broadband modulating capability in visible, NIR, and MIR region, enabling the SPWs distinguished energy-saving effect in both hot and cold seasons. Our concept could create a broad prospect for real-world application of ESBs, and push forward the realization of the target of carbon neutrality and social sustainable development.

Acknowledgements This project was supported by Natural Science Foundation of China (Grant No. 52372076, 52073081, 52203322, 5252200843), Ministry of Science and Technology of the People's Republic of China (2023YFB3812800) and Fundamental Research Funds for the Central Universities (FRF-TP-25-073).

Author Contributions Qian Wang was involved in conceptualization, investigation, and writing—review and editing; Zongxu Na was responsible for conducting a research and investigation process, formal analysis, visualization, and writing—original draft; Jianfei Gao contributed to validation and formal analysis; Li Yu took part in conceptualization, supervision, validation, formal analysis, and data curation; Yuanwei Chen was responsible for conceptualization and data curation; Peng Gao took part in

data curation; Yong Ding was responsible for investigation and resources; Songyuan Dai took part in supervision; Mohammad Khaja Nazeeruddin was involved in conceptualization and project administration; Huai Yang was responsible for conceptualization, funding acquisition, and supervision.

Declarations

Conflict of interest The authors declare no conflict of interest. They have no known competing financial interests or personal relationships that could have appeared to influence the work reported in this paper. All authors declare that there are no competing interests.

Supplementary Information The online version contains supplementary material available at https://doi.org/10.1007/s40820-025-01985-w.

References

1. J. Chai, J. Fan, Solar and thermal radiation-modulation materials for building applications. Adv. Energy Mater. **13**(1), 2202932 (2023). https://doi.org/10.1002/aenm.202202932
2. C.Z. Li, L. Zhang, X. Liang, B. Xiao, V.W.Y. Tam et al., Advances in the research of building energy saving. Energy Build. **254**, 111556 (2022). https://doi.org/10.1016/j.enbuild.2021.111556
3. A.M. Omer, Energy, environment and sustainable development. Renew. Sustain. Energy Rev. **12**(9), 2265–2300 (2008). https://doi.org/10.1016/j.rser.2007.05.001
4. S. Jia, Q. Weng, C. Yoo, H. Xiao, Q. Zhong, Building energy savings by green roofs and cool roofs in current and future climates. NPJ Urban Sustain. **4**, 23 (2024). https://doi.org/10.1038/s42949-024-00159-8
5. L. Long, H. Ye, How to be smart and energy efficient: a general discussion on thermochromic windows. Sci. Rep. **4**, 6427 (2014). https://doi.org/10.1038/srep06427
6. W.J. Hee, M.A. Alghoul, B. Bakhtyar, O. Elayeb, M.A. Shameri et al., The role of window glazing on daylighting and energy saving in buildings. Renew. Sustain. Energy Rev. **42**, 323–343 (2015). https://doi.org/10.1016/j.rser.2014.09.020
7. Z. Duan, S. Wu, H. Sun, B. Lin, P. Ding et al., Improvements in energy saving and thermal comfort for electric vehicles in summer through coupled electrochromic and radiative cooling smart windows. Build. Simul. **17**(8), 1231–1251 (2024). https://doi.org/10.1007/s12273-024-1137-2
8. N.C. Davy, M. Sezen-Edmonds, J. Gao, X. Lin, A. Liu et al., Pairing of near-ultraviolet solar cells with electrochromic windows for smart management of the solar spectrum. Nat. Energy **2**, 17104 (2017). https://doi.org/10.1038/nenergy.2017.104
9. H. Li, W. Zhang, A.Y. Elezzabi, Transparent zinc-mesh electrodes for solar-charging electrochromic windows. Adv. Mater. **32**(43), e2003574 (2020). https://doi.org/10.1002/adma.202003574
10. Z. Kou, J. Wang, X. Tong, P. Lei, Y. Gao et al., Multi-functional electrochromic energy storage smart window powered by CZTSSe solar cell for intelligent managing solar radiation of building. Sol. Energy Mater. Sol. Cells **254**, 112273 (2023). https://doi.org/10.1016/j.solmat.2023.112273
11. Y. Meng, Y. Tan, X. Li, Y. Cai, J. Peng et al., Building-integrated photovoltaic smart window with energy generation and conservation. Appl. Energy **324**, 119676 (2022). https://doi.org/10.1016/j.apenergy.2022.119676
12. G. Syrrokostas, G. Leftheriotis, S.N. Yannopoulos, Lessons learned from 25 years of development of photoelectrochromic devices: a technical review. Renew. Sustain. Energy Rev. **162**, 112462 (2022). https://doi.org/10.1016/j.rser.2022.112462
13. Z. Liu, J. Yang, G. Leftheriotis, H. Huang, Y. Xia et al., A solar-powered multifunctional and multimode electrochromic smart window based on WO_3/Prussian blue complementary structure. Sustain. Mater. Technol. **31**, e00372 (2022). https://doi.org/10.1016/j.susmat.2021.e00372
14. Z. Wang, X. Jia, P. Zhang, Y. Liu, H. Qi et al., Viologen-immobilized 2D polymer film enabling highly efficient electrochromic device for solar-powered smart window. Adv. Mater. **34**(1), 2106073 (2022). https://doi.org/10.1002/adma.202106073
15. Y. Liang, S. Cao, Q. Wei, R. Zeng, J. Zhao et al., Reversible Zn^{2+} insertion in tungsten ion-activated titanium dioxide nanocrystals for electrochromic windows. Nano-Micro Lett. **13**(1), 196 (2021). https://doi.org/10.1007/s40820-021-00719-y
16. P. Lei, J. Wang, Y. Gao, C. Hu, S. Zhang et al., An electrochromic nickel phosphate film for large-area smart window with ultra-large optical modulation. Nano-Micro Lett. **15**(1), 34 (2023). https://doi.org/10.1007/s40820-022-01002-4
17. Z. Zhang, M. Yu, C. Ma, L. He, X. He et al., A Janus smart window for temperature-adaptive radiative cooling and adjustable solar transmittance. Nano-Micro Lett. **17**(1), 233 (2025). https://doi.org/10.1007/s40820-025-01740-1
18. C.-Y. Cheng, Y.-J. Chiang, H.-F. Yu, L.-Y. Hsiao, C.-L. Yeh et al., Designing a hybrid type photoelectrochromic device with dual coloring modes for realizing ultrafast response/high optical contrast self-powered smart windows. Nano Energy **90**, 106575 (2021). https://doi.org/10.1016/j.nanoen.2021.106575

19. C.J. Barile, D.J. Slotcavage, J. Hou, M.T. Strand, T.S. Hernandez et al., Dynamic windows with neutral color, high contrast, and excellent durability using reversible metal electrodeposition. Joule **1**(1), 133–145 (2017). https://doi.org/10.1016/j.joule.2017.06.001
20. S. Yang, J. Zheng, M. Li, C. Xu, A novel photoelectrochromic device based on poly(3, 4-(2, 2-dimethylpropylenedioxy)thiophene) thin film and dye-sensitized solar cell. Sol. Energy Mater. Sol. Cells **97**, 186–190 (2012). https://doi.org/10.1016/j.solmat.2011.09.038
21. C.-L. Lin, C.-Y. Chen, H.-F. Yu, K.-C. Ho, Comparisons of the electrochromic properties of poly(hydroxymethyl 3, 4-ethylenedioxythiophene) and poly(3, 4-ethylenedioxythiophene) thin films and the photoelectrochromic devices using these thin films. Sol. Energy Mater. Sol. Cells **202**, 110132 (2019). https://doi.org/10.1016/j.solmat.2019.110132
22. Y. Liu, J. Wang, F. Wang, Z. Cheng, Y. Fang et al., Full-frame and high-contrast smart windows from halide-exchanged perovskites. Nat. Commun. **12**(1), 3360 (2021). https://doi.org/10.1038/s41467-021-23701-z
23. H. Ling, J. Wu, F. Su, Y. Tian, Y.J. Liu, Automatic light-adjusting electrochromic device powered by perovskite solar cell. Nat. Commun. **12**(1), 1010 (2021). https://doi.org/10.1038/s41467-021-21086-7
24. L. Lavagna, G. Syrrokostas, L. Fagiolari, J. Amici, C. Francia et al., Platinum-free photoelectrochromic devices working with copper-based electrolytes for ultrastable smart windows. J. Mater. Chem. A **9**(35), 19687–19691 (2021). https://doi.org/10.1039/D1TA03544D
25. M.K. Ganesha, I. Mondal, A.K. Singh, G.U. Kulkarni, Fabrication of large-area, affordable dual-function electrochromic smart windows by using a hybrid electrode coated with an oxygen-deficient tungsten oxide ultrathin porous film. ACS Appl. Mater. Interfaces **15**(15), 19111–19120 (2023). https://doi.org/10.1021/acsami.2c22638
26. I. Mondal, M.K. Ganesha, A.K. Singh, G.U. Kulkarni, Affordable smart windows with dual-functionality: electrochromic color switching and charge storage. Adv. Mater. Technol. **8**(18), 2300651 (2023). https://doi.org/10.1002/admt.202300651
27. Z. Xu, W. Li, J. Huang, X. Guo, Q. Liu et al., Flexible, controllable and angle-independent photoelectrochromic display enabled by smart sunlight management. Nano Energy **63**, 103830 (2019). https://doi.org/10.1016/j.nanoen.2019.06.026
28. M.K. Ganesha, H. Hakkeem, I. Mondal, A.K. Singh, G.U. Kulkarni, An ITO free all tungsten-based electrochromic energy storage device as smart window. Small **20**(48), 2405467 (2024). https://doi.org/10.1002/smll.202405467
29. M.K. Ganesha, H. Hakkeem, A.K. Singh, Redox potential based self-powered electrochromic devices for smart windows. Small **20**(42), e2403156 (2024). https://doi.org/10.1002/smll.202403156
30. R. Roy, R. Greeshma, A. Basith, R. Banerjee, A.K. Singh, Self-rechargeable aqueous Zn^{2+}/K^{+} electrochromic energy storage device *via* scalable spray-coating integrated with Marangoni flow. Energy Storage Mater. **71**, 103680 (2024). https://doi.org/10.1016/j.ensm.2024.103680
31. Y. Xia, X. Liang, Y. Jiang, S. Wang, Y. Qi et al., High-efficiency and reliable smart photovoltaic windows enabled by multiresponsive liquid crystal composite films and semi-transparent perovskite solar cells. Adv. Energy Mater. **9**(33), 1900720 (2019). https://doi.org/10.1002/aenm.201900720
32. Z. Na, X. Liang, H. Wang, L. Yu, C. Fan et al., Broadband modulation, self-driven, and self-cleaning smart photovoltaic windows for high efficiency energy saving buildings. Adv. Funct. Mater. **34**(2), 2308312 (2024). https://doi.org/10.1002/adfm.202308312
33. S. Agarwal, S. Srivastava, S. Joshi, S. Tripathi, B.P. Singh et al., A comprehensive review on polymer-dispersed liquid crystals: mechanisms, materials, and applications. ACS Mater. Au **5**(1), 88–114 (2025). https://doi.org/10.1021/acsmaterialsau.4c00122
34. S. Shaik, K. Gorantla, M. Venkata Ramana, S. Mishra, K.S. Kulkarni, Thermal and cost assessment of various polymer-dispersed liquid crystal film smart windows for energy efficient buildings. Constr. Build. Mater. **263**, 120155 (2020). https://doi.org/10.1016/j.conbuildmat.2020.120155
35. H. Shim, H.-K. Lyu, B. Allabergenov, Y. Garbovskiy, A. Glushchenko et al., Switchable response of ferroelectric nanoparticle doped polymer-dispersed liquid crystals. J. Nanosci. Nanotechnol. **16**(10), 11125–11129 (2016). https://doi.org/10.1166/jnn.2016.13302
36. Z. Liang, Y. Zhao, H. Gao, D. Wang, Z. Miao et al., Influence of ZnO NPs on morphological and electro-optical properties of polymer-dispersed liquid crystals. Liq. Cryst. **48**(12), 1699–1708 (2021). https://doi.org/10.1080/02678292.2021.1898055
37. M. Ellahi, J. Muhammad, M. Furqan Ali, K.H. Mangi, A.M. Bhayo et al., Preparation of silver nanoparticles (AgNPs)-doped epoxy-based thin PDLC films (smart glass). Polym. Bull. **79**(5), 3135–3153 (2022). https://doi.org/10.1007/s00289-021-03670-5
38. X. Zhao, M. Sheng, H. Tang, H. Pan, C. Guo et al., A flexible electrochromic device for all-season thermal regulation on curved transparent building envelopes. ACS Appl. Mater. Interfaces **16**(32), 42481–42490 (2024). https://doi.org/10.1021/acsami.4c08207
39. Y. Huang, S. Wu, S. Zhao, Z. Guo, Z. Zhao et al., A novel liquid flow electrochromic smart window for all-year-round dynamic photothermal regulation. Energy Environ. Sci. **18**(4), 1824–1834 (2025). https://doi.org/10.1039/d4ee05416d
40. Z. Shao, A. Huang, C. Cao, X. Ji, W. Hu et al., Tri-band electrochromic smart window for energy savings in buildings. Nat. Sustain. **7**(6), 796–803 (2024). https://doi.org/10.1038/s41893-024-01349-z
41. Z. Zhang, Y. Yang, C. Ma, M. Yu, J. Xu et al., Enhanced electro-optical and heat regulation of intelligent dimming films using the photovoltaic effect of *p–n* heterostructures. Adv. Funct. Mater. **34**(45), 2406858 (2024). https://doi.org/10.1002/adfm.202406858

42. Y. Deng, Y. Yang, Y. Xiao, H.-L. Xie, R. Lan et al., Ultrafast switchable passive radiative cooling smart windows with synergistic optical modulation. Adv. Funct. Mater. **33**(35), 2301319 (2023). https://doi.org/10.1002/adfm.202301319
43. Y. Deng, Y. Yang, Y. Xiao, X. Zeng, H.-L. Xie et al., Annual energy-saving smart windows with actively controllable passive radiative cooling and multimode heating regulation. Adv. Mater. **36**(27), 2401869 (2024). https://doi.org/10.1002/adma.202401869
44. S. Wu, Y. Wang, M. Iqbal, K. Mehmood, Y. Li et al., Challenges of fluoride pollution in environment: mechanisms and pathological significance of toxicity—a review. Environ. Pollut. **304**, 119241 (2022). https://doi.org/10.1016/j.envpol.2022.119241
45. Y. Zhai, Y. Ma, S.N. David, D. Zhao, R. Lou et al., Scalable-manufactured randomized glass-polymer hybrid metamaterial for daytime radiative cooling. Science **355**(6329), 1062–1066 (2017). https://doi.org/10.1126/science.aai7899
46. Y. Zhang, J. Yu, *In situ* formation of SiO_2 nanospheres on common fabrics for broadband radiative cooling. ACS Appl. Nano Mater. **4**(10), 11260–11268 (2021). https://doi.org/10.1021/acsanm.1c02841
47. S. Lin, H. Wang, X. Zhang, D. Wang, D. Zu et al., Direct spray-coating of highly robust and transparent Ag nanowires for energy saving windows. Nano Energy **62**, 111–116 (2019). https://doi.org/10.1016/j.nanoen.2019.04.071
48. H. Zhang, Z. Miao, W. Shen, Development of polymer-dispersed liquid crystals: from mode innovation to applications. Compos. Part A Appl. Sci. Manuf. **163**, 107234 (2022). https://doi.org/10.1016/j.compositesa.2022.107234
49. N. Nasir, S. Kumar, M. Kim, V.H. Nguyen, M. Suleman et al., Effect of the photoinitiator concentration on the electro-optical properties of thiol–acrylate-based PDLC smart windows. ACS Appl. Energy Mater. **5**(6), 6986–6995 (2022). https://doi.org/10.1021/acsaem.2c00623
50. G.P. Montgomery Jr., J.L. West, W. Tamura-Lis, Light scattering from polymer-dispersed liquid crystal films: droplet size effects. J. Appl. Phys. **69**(3), 1605–1612 (1991). https://doi.org/10.1063/1.347256
51. M. Kim, K.J. Park, S. Seok, J.M. Ok, H.-T. Jung et al., Fabrication of microcapsules for dye-doped polymer-dispersed liquid crystal-based smart windows. ACS Appl. Mater. Interfaces **7**(32), 17904–17909 (2015). https://doi.org/10.1021/acsami.5b04496
52. M. Yu, J. Xu, L. Luo, L. Zhang, Y. Gao et al., Role of hydroxy group in the electro-optical properties of polymer-dispersed liquid crystals. Crystals **13**(5), 843 (2023). https://doi.org/10.3390/cryst13050843
53. W. Li, L. Yu, W. He, X. Yuan, D. Zhao et al., Effect of a photopolymerizable monomer containing a hydrogen bond on near-infrared radiation transmittance of nematic liquid crystal/monomers composites. J. Phys. Chem. C **112**(35), 13739–13743 (2008). https://doi.org/10.1021/jp804490b
54. M. Yu, F. Zhou, L. Zhang, X. He, C. Chen et al., Effects of hydroxylated acrylates on electro-optical performance and adhesion strength of polymer dispersed liquid crystal films. J. Mol. Liq. **397**, 124180 (2024). https://doi.org/10.1016/j.molliq.2024.124180
55. Z. He, P. Yu, Y. Zhao, Q. Yang, Y. Zhao et al., The regulation of electric-optical properties of polymer-dispersed liquid crystals *via* implantation of polyhedral oligomeric silsesquioxane (POSS) microstructure. Liq. Cryst. **49**(2), 240–247 (2022). https://doi.org/10.1080/02678292.2021.1956611
56. Z. He, P. Yu, H. Zhang, Y. Zhao, Y. Zhu et al., Silicon nanostructure-doped polymer/nematic liquid crystal composites for low voltage-driven smart windows. Nanotechnology **33**(8), 085205 (2022). https://doi.org/10.1088/1361-6528/ac3a3b
57. Z. Ding, X. Li, Q. Ji, Y. Zhang, H. Li et al., Machine-learning-assisted design of a robust biomimetic radiative cooling metamaterial. ACS Mater. Lett. **6**(6), 2416–2424 (2024). https://doi.org/10.1021/acsmaterialslett.4c00337
58. Z. Ding, H. Li, X. Li, X. Fan, J. Jaramillo-Fernandez et al., Designer SiO_2 metasurfaces for efficient passive radiative cooling. Adv. Mater. Interfaces **11**(3), 2300603 (2024). https://doi.org/10.1002/admi.202300603
59. J. Atkinson, I.A. Goldthorpe, Near-infrared properties of silver nanowire networks. Nanotechnology **31**(36), 365201 (2020). https://doi.org/10.1088/1361-6528/ab94de
60. H. Hu, S. Wang, Y. Meng, G. Liu, M. Li et al., Layer-by-layer alignment of silver nanowires for transparent and flexible energy-saving windows. Adv. Mater. Technol. **7**(3), 2100824 (2022). https://doi.org/10.1002/admt.202100824
61. K. Jiang, K. Zhang, Z. Shi, H. Li, B. Wu et al., Experimental and numerical study on the potential of a new radiative cooling paint boosted by SiO_2 microparticles for energy saving. Energy **283**, 128473 (2023). https://doi.org/10.1016/j.energy.2023.128473
62. S. Hanauer, C. Celle, C. Crivello, H. Szambolics, D. Muñoz-Rojas et al., Transparent and mechanically resistant silver-nanowire-based low-emissivity coatings. ACS Appl. Mater. Interfaces **13**(18), 21971–21978 (2021). https://doi.org/10.1021/acsami.1c02689
63. C. Lin, J. Hur, C.Y.H. Chao, G. Liu, S. Yao et al., All-weather thermochromic windows for synchronous solar and thermal radiation regulation. Sci. Adv. **8**(17), eabn7359 (2022). https://doi.org/10.1126/sciadv.abn7359

 https://doi.org/10.1007/s40820-025-01985-w